AD-A074 408 NAVY ELECTRONICS LAB SAN DIEGO CA F/G 17/1
THE REFLECTION OF LOW FREQUENCY SONAR SIGNALS FROM A SMOOTH OCE--ETC(U)
1963 H P BUCKER

UNCLASSIFIED NL

| OF |
AD A074408

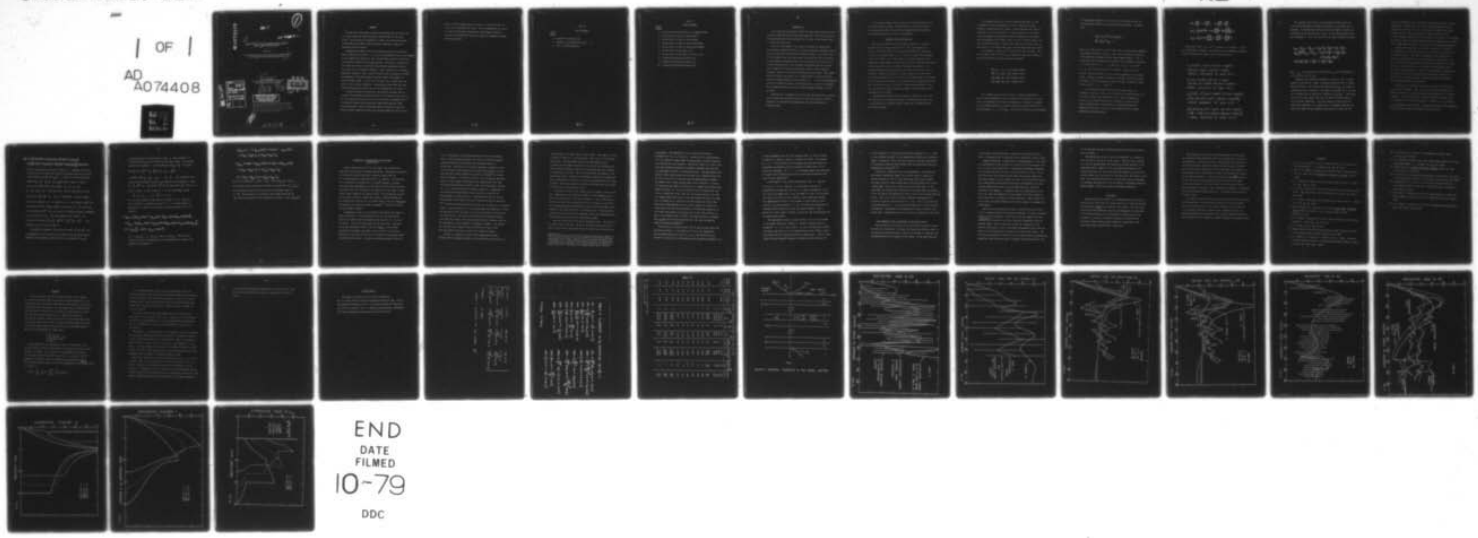

END
DATE FILMED
10-79
DDC

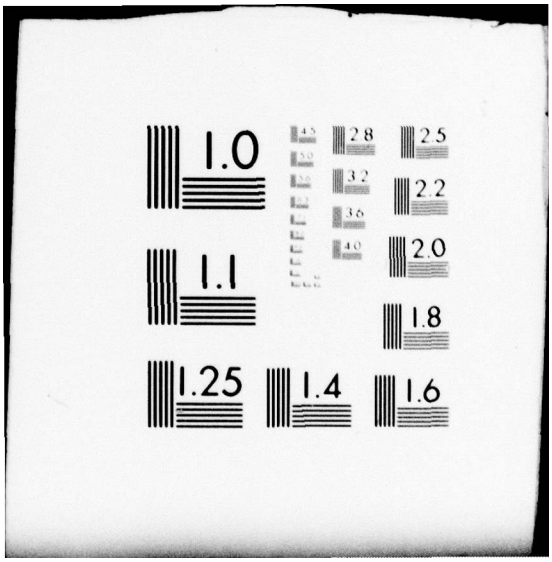
1.0
1.1
1.25
1.4
1.6
1.8
2.0
2.2
2.5
2.8
3.2
3.6
4.0
4.5
5.0

AD A074408

LEVEL III

MOST Project 3-2

THE REFLECTION OF LOW FREQUENCY SONAR SIGNALS FROM A SMOOTH OCEAN BOTTOM

Part II

Calculations of Bottom Losses for a Layered Model and Comparison with Experimental Values

by

H. P. Bucker
U. S. Navy Electronics Laboratory
San Diego, California 92152

1963

13 p.

DDC FILE COPY

ACCESSION for
NTIS White Section
DDC Buff Section
UNANNOUNCED
JUSTIFICATION Per Letter on File
BY
DISTRIBUTION/AVAILABILITY CODES
Dist. AVAIL. and/or SPECIAL
A

DDC
RECEIVED
APR 2 1979
F

DISTRIBUTION STATEMENT A
Approved for public release;
Distribution Unlimited

The opinions and assertions contained herein are the private ones of the writer, and are not to be construed as official, or as reflecting the views of the Navy Department or the naval service at large.

253 550

ABSTRACT

In Part II of this paper, calculations are made for the bottom loss of a plane sound wave reflecting from a layered model of the ocean bottom. The sea floor is considered to consist of an arbitrary number of absorbing solid layers, each of constant thickness, lying on an absorbing solid half-space.

Comparisons are made between the calculated losses and the experimental values given in Part I. In one of the experimental areas a core sample of the sediment was obtained so that a bottom model could be constructed to accurately represent the in situ layering. Attenuation constants for this model were chosen so that the calculated and experimental bottom loss curves are in reasonable agreement. These constants are in general agreement, assuming a linear relation between sound attenuation (in db/ft) and frequency, with high frequency resonant chamber measurements on similar sediment types. In the other two areas less is known about the nature of the sea floor sediments. Bottom models constructed for these areas provide possible explanations of the experimental loss curves.

A short discussion of bottom loss fluctuations concludes Part II. A study of the possible sound paths leads to the conclusion that most of the fluctuations observed in two of the three areas are probably due to interference between the four possible signal paths having a single bottom reflection. These fluctuations should be expected in any test where the pulse lengths and source and receiver depths are such that the

bottom reflected signals are not resolved. At the third area the bottom loss fluctuations are large. This is most probably the result of combining experimental measurements from slightly different locations in an area where there are strong, but somewhat irregular, reflecting surfaces.

Part II

LIST OF TABLES

Part II

LIST OF FIGURES

Figure Number

INTRODUCTION

If a sound wave is projected toward the ocean bottom there will be a specularly reflected wave of diminished amplitude. The ratio (in db) of the sound intensity of this reflected wave to that of the incident wave is called the bottom loss.

Part II of this paper is an attempt to explain the experimental bottom losses reported in Part I, in terms of available information about the test conditions and the bottom sediments present in the three areas. For this purpose, the first and largest section of Part II is devoted to the development of equations which can be solved for the bottom loss of a plane sinusoidal wave in an isotropic liquid half-space and incident upon a number of isotropic absorbing solid layers, each of constant thickness, lying on an isotropic absorbing solid half-space. This sample model has obvious limitations in its representation of any real bottom reflection problem, however, in most cases it would serve as an approximate solution to which the effects of scattering, deviations due to non-plane wave fronts, non-sinusoidal signals, uneven sediment layering, etc. can be added.

Following the development of equations for the bottom loss, calculations are made for the areas discussed in the second section of Part I. Comparison of calculated and experimental values are presented in graphical form.

In the third section a brief discussion of the fluctuation of the bottom loss values is given. The experimental fluctuations measured in the deep water areas (II and III) are compared with the expected four-signal fluctuation, derived in the Appendix.

EQUATIONS FOR THE BOTTOM LOSS

The ocean bottom has been traditionally treated as a liquid in problems involving bottom reflection[1,2]. When the absorption of sound in the bottom needs to be considered, and when this absorption is small, a convenient model to use is that of a liquid with a complex velocity of sound[3]. In a recent paper, T. G. Bell[4] reported on the comparison of experimental bottom losses in several areas with theoretical values calculated using a two-layer "absorbing" liquid model. The agreement between the calculated and observed values of bottom loss is excellent. However, the neglect in these studies of the shear waves that would be generated in the viscous liquid layers might be questioned, since in several of the models the attenuation of the compressional wave was of the order of 0.3 - 0.6 db/ft. A more realistic model is that of a visco-elastic solid[5] in which the effects of bottom rigidity and absorption are included.

The problem of calculating the reflection coefficient of a sound wave incident on a visco-elastic layer is essentially the same as for a wave incident on an elastic layer[6], except that the Lamé constants are complex numbers.

It is assumed here that an area of ocean bottom which is under consideration can be represented as a set of isotropic, constant thickness, visco-elastic solid layers. The bottom layer has infinite thickness, i.e. it is a half-space. A plane sound wave in the water layer and incident on this model bottom will generate in each layer, with the exception of the lowest layer, four sets of plane waves, two sets of up-and-down going compressional waves and two similar sets of shear waves. In the bottom layer only the down-going waves are present.

As in Figure 1, denote the n^{th} layer by the same subscript. The sets of waves in the n^{th} layer can be defined, in the usual manner, in terms of four scalar velocity potential functions[7]:

$$\Phi_n' = A_n' \exp. i(kx + a_n kz - \omega t),$$
$$\Phi_n'' = A_n'' \exp. i(kx - a_n kz - \omega t),$$
$$\psi_n' = B_n' \exp. i(kx + b_n kz - \omega t),$$
$$\psi_n'' = B_n'' \exp. i(kx - b_n kz - \omega t).$$

It is assumed that only real values of k need be considered to obtain a good approximation to the incident wave in the water. In this case k is determined by the angular frequency ω, the angle of incidence of the incoming sound wave θ_i, and the velocity of sound in the water c_w by the relation $k = \omega \sin \theta_i / c_w$. The values of a_n and b_n are determined

by the physical properties of the layer and the condition that the potentials must satisfy their respective wave equations. It follows that:

$$a_n^2 = \left[\rho_n c^2 / (\lambda_n + 2\mu_n) \right] - 1,$$

$$b_n^2 = \left[\rho_n c^2 / \mu_n \right] - 1.$$

Here, ρ_n is the density of the n^{th} layer and c, the horizontal component of the phase velocity, is equal to ω/k. The visco-elastic properties of the layer are determined by the complex Lamé constants λ and μ. Consistent with the assumed time dependence of the potential functions, λ_n can be written as $\lambda_n' - i\lambda_n''$ and μ_n as $\mu_n' - i\mu_n''$ where λ_n', λ_n'', μ_n' and μ_n'' are positive real numbers. The roots of a_n^2 and b_n^2 should be chosen to lie in the first quadrant of the complex plane. In order to reduce the number of constants required to define the model it will be assumed here that the volume viscosity is equal to zero, that is, $\lambda_n'' = -2\mu_n'' / 3$.

At the interface between the two visco-elastic layers the components of particle velocity in the vertical (z) and horizontal (x) directions, respectively denoted by w and u, and the elements p_{zz} and p_{xz} of the stress tensor must be continuous. In the case of plane sinusoidal waves, assumed here, the relations between the component velocities, the stress tensor elements and the velocity potentials can be written as:

$$W = \frac{\partial \Phi}{\partial z} + \frac{\partial \Psi}{\partial x}, \quad u = \frac{\partial \Phi}{\partial x} - \frac{\partial \Psi}{\partial z},$$

$$p_{zz} = \frac{i}{\omega}\left(-\rho\omega^2\Phi - 2\mu \frac{\partial^2 \Phi}{\partial x^2} + 2\mu \frac{\partial^2 \Psi}{\partial x \partial z}\right),$$

$$p_{xz} = \frac{i}{\omega}\mu\left(2 \frac{\partial^2 \Phi}{\partial x \partial z} + \frac{\partial^2 \Psi}{\partial x^2} - \frac{\partial^2 \Psi}{\partial z^2}\right).$$

Referring to Fig. 1 let the n^{th} interface be a distance h below the water-sediment interface. It follows that the interface conditions at the n^{th} interface (at depth $z=h$) can be written as:

$$a_n \left[A'_n \exp. i\,(a_n kh) - A''_n \exp. i\,(-a_n kh)\right]$$
$$+ B'_n \exp. i\,(b_n kh) + B''_n \exp. i\,(-b_n kh)$$
$$= \text{similar expression for layer } (n+1).$$

$$A'_n \exp. i\,(a_n kh) + A''_n \exp. i\,(-a_n kh)$$
$$- b_n \left[B'_n \exp. i\,(b_n kh) - B''_n \exp. i\,(-b_n kh)\right]$$
$$= \text{similar expression for layer } (n+1).$$

$$\mu_n \Big\{(b_n^2 - 1)\left[A'_n \exp. i\,(a_n kh) + A''_n \exp. i\,(-a_n kh)\right]$$
$$+ 2 b_n \left[B'_n \exp. i\,(b_n kh) - B''_n \exp. i\,(-b_n kh)\right]\Big\}$$
$$= \text{similar expression for layer } (n+1).$$

$$\mu_n \Big\{-2 a_n \left[A'_n \exp. i\,(a_n kh) - A''_n \exp. i\,(-a_n kh)\right]$$
$$+ (b_n^2 - 1)\left[B'_n \exp. i\,(b_n kh) + B''_n \exp. i\,(-b_n kh)\right]\Big\}$$
$$= \text{simiar expression for layer } (n+1).$$

The equations valid at the other interfaces between layers can be obtained by appropriate change of subscripts and the depth of the interface. In the equations associated with the deepest interface the coefficients A''_1 and B''_1 are equal to zero. At the water-sediment interface (interface p at z = 0), there are only three interface equations:

$$a_{p+1}\,(A'_{p+1} - A''_{p+1}) = a_p(A'_p - A''_p) + (B'_n + B''_n),$$

$$\rho_{p+1}\left(\frac{\omega}{k}\right)^2(A'_{p+1} + A''_{p+1}) = \mu_p\left[(b_p^2 - 1)(A'_p + A''_p) + 2b_p(B'_p - B''_p)\right],$$

$$2a_p(A'_p - A''_p) = (b_p^2 - 1)(B'_p + B''_p),$$

Here, ρ_{p+1} is the density of the water and a_{p+1} can be identified as $\cot\theta_i$ and k as $\omega \sin\theta_i / c_w$.

In general the interface conditions will result in 4N + 3 linear algebraic equations (N = number of layers) relating the 4N + 4 complex amplitude factors. By dividing each equation with A'_{p+1} the number of unknown quantities is reduced to the number of equations and a solution can be obtained for the reflection coefficient A''_{p+1}/A'_{p+1}. The bottom loss in db is minus twenty times the log (base 10) of the modulus of the reflection coefficient. One direct method of solution for the reflection coefficient is to expand the set of complex equations into twice that number of real algebraic equations and to solve for the

reflection coefficient by an iterative inversion of the matrix of real coefficients. However, when the number of layers becomes large the computation time required to set up and invert the coefficient matrix becomes excessive (the time required to invert a matrix in most iterative methods increases as the third power of the order of the matrix). An efficient method of calculating the reflection coefficient for a model with a large number of layers is developed in the following paragraphs.

From physical arguments, the stresses and particle velocities at one interface of a layer are related to the stresses and velocities at the second interface. For small displacements these relations are linear and can be expressed as a matrix equation. This method is due to W. T. Thomson[8] who calculated the reflection coefficient of a plane wave in a liquid incident on a set of elastic solid layers bounded below by a liquid half-space. Here the same procedure is followed, but each layer and the lower half-space are assumed to be visco-elastic solids. Also, a minor correction to Thomson's equations concerning the interface conditions has been made.

Let u_n^m be the x component of particle velocity in the n^{th} layer and at the m^{th} interface. Here and in later parts of this paper subscripts will refer to a particular layer and superscripts to a specific interface. Let the origin of the coordinate system be shifted to the n-1 interface so that the n^{th} interface is located at $z = -d_n$, where d_n is the thickness of the n^{th} layer. From previous equations the expression of u_n^n, with the time factor omitted, can be written as:

$$u_n^n = ik\left\{\left[A'_n \exp.i(-a_n k_n d_n) + A''_n \exp.i(a_n k_n d_n)\right] - b_n\left[B'_n \exp.i(-b_n k_n d_n) - B''_n \exp.i(b_n k_n d_n)\right]\right\} \exp.i(kx).$$

Similar equations can be written for w_n^n, the z component of particle velocity in the n^{th} layer and at the n^{th} interface, and for the stress tensor elements $(p_{zz})_n^n$ and $(p_{xz})_n^n$. Let V_n^m be a column matrix with elements u_n^m, w_n^m, $(p_{zz})_n^m$, and $(p_{xz})_n^m$, where m may be n or n-1. Let W_n be a column matrix with elements $A'_n + A''_n$, $A'_n - A''_n$, $B'_n - B''_n$ and $B'_n + B''_n$. Then V_n^m and W_n can be connected by a matrix equation; let $V_n^m = M_n^m \cdot W_n$. The 4 x 4 matrix M_n^n is given in Table 1. Because the interface n-1 is located at z = 0 the elements of M_n^{n-1} can be obtained from the elements of M_n^n by setting $d_n = 0$. Note that half of the elements of M_n^{n-1} are zero because of the plus and minus arrangement of the A's and B's in W_n. The column matrices V_n^n and V_n^{n-1} are related by the equation $V_n^n = M_n^n \cdot [M_n^{n-1}]^{-1} \cdot V_n^{n-1} \equiv D_n \cdot V_n^{n-1}$. The elements of D_n are listed in Table 2.

From physical arguments, the relations between V_n^n and V_n^{n-1} must be independent of the location of the origin of the coordinate system. Therefore, the quantity d_n, which occurs in the elements of D_n, has

significance only as the thickness of layer n. Thus, matrices of the same form as D_n can be written for the other layers. The boundary condition at interface n can be expressed as $V^n_{n+1} = V^n_n$. It follows that $V^p_p = D_p \cdot V^{p-1}_p = D_p \cdot V^{p-1}_{p-1} = D_p \cdot D_{p-1} \cdot V^{p-2}_{p-1} = \ldots$,

or finally, $V^p_p = D_p \cdot D_{p-1} \cdot D_{p-2} \ldots D_2 \cdot V^1_2$. For convenience, the origin of the coordinate system is now shifted to the interface 1. Then, $V^1_2 = V^1_1 = M^{1*}_1 \cdot W_1$. The matrix M^{1*}_1 has the same form as M^n_n with $d_n = 0$, because surface 1 is now located at z = 0. For convenience, define

$$V^p_p = D_p \cdot D_{p-1} \ldots D_2 \cdot M^{1*}_1 \cdot W_1 \equiv F \cdot W_1.$$

Let the total thickness of the layers 2 through p be H. The water-solid interface is, therefore, located at z = -H. Noting that the p-1 half-space is a liquid, the following interface conditions hold at the surface p:

$$i a_{p+1} k \left[A'_{p+1} \exp. i(-a_{p+1} kH) - A''_{p+1} \exp. i(a_{p+1} kH) \right] = W^p_p,$$

$$-i \rho_{p+1} \omega \left[A'_{p+1} \exp. i(-a_{p+1} kH) + A''_{p+1} \exp. i(a_{p+1} kH) \right] = (p_{zz})^p_p,$$

$$0 = (p_{xz})^p_p, \text{ here } a_{p+1} = \cos \theta_i$$

Let $R = A''_{p+1}/A'_{p+1}$, $T_c = A'_1/A'_{p+1}$, and $T_s = B'_1/A'_{p+1}$. The preceding equations can then be expanded into the following form in terms of the elements of the matrix F.

$$i a_{p+1} k \exp. i(-a_{p+1} kH)\left[1 - R \exp. i(a_{p+1} kH)\right]$$

$$= (F_{21} + F_{22})\, T_c + (F_{23} + F_{24})\, T_s ,$$

$$-i\rho_{p+1}\, \omega \exp. i\,(-a_{p+1} kH)\left[1 + R \exp. i\,(2a_{p+1} kH)\right]$$

$$= (F_{31} + F_{32})\, T_c + (F_{33} + F_{34})\, T_s ,$$

$$0 = (F_{41} + F_{42})\, T_c + (F_{43} + F_{44})\, T_s .$$

This set of equations is solved to find $R \exp.i(2a_{p+1}kH)$, which is the desired ratio of reflected-to-incident sound pressure (A''_{p+1}/A'_{p+1}) at the interface between the water and the top sediment layer (at $z = -H$). The bottom loss is defined as minus twenty times the log (base 10) of the modulus of the reflection coefficient $R \exp i(2a_{p+1}kH)$.

COMPARISON OF EXPERIMENTAL AND CALCULATED BOTTOM LOSSES

Area I, discussed in Part I of this paper, lies in moderately deep water off the coast of Southern California. The physical properties of the bottom in Area I have been studied by a group from the U. S. Navy Electronics Laboratory under E. L. Hamilton. Low frequency sub-bottom profile recordings by D. G. Moore[9] indicate a strongly reflecting layer approximately 20 feet below the water-bottom interface. As noted in Part I of this paper, the composition of the upper sediment layers varies throughout the operating area. The bottom model assumed in this area is based on several core samples, obtained by Hamilton. The compressional velocities in the layers found in the core samples were determined by the resonance method of Shumway[10, 11] and are listed in column 9, Table 3, Model A.

A mathematical model of the bottom was then constructed (Table 3, Model A) for Area I. The experimental values of the velocity and density of a layer essentially determine the value of $(\lambda' + 2\mu')$ for the layer[5]. A value was then chosen for the ratio μ'/λ' according to the type of material found in the core samples. In the models described in this paper, the choice of this ratio is not critical. Variations in the value of (μ'/λ') of the order of 0.1 has small effect on the bottom loss curves. It may be noted that choosing a value for

μ'/λ' is equivalent to specifying Poisson's ratio for the sediment layer. The attenuation constants were chosen to provide reasonable agreement between the experimental and calculated values of bottom loss. The values are in general agreement, assuming a linear relation between sound absorption (in db/ft) and frequency, with the high frequency resonant chamber measurements of Shumway[10] on similar types of sediment. In contrast, however, these attenuation constants result in a much higher attenuation of the compressional wave than that measured by Wood and Weston[12] in mud. The bottom model constants (λ', μ', μ'', and ρ) are listed in Table 3, Model A. A comparison of the calculated and experimental bottom losses, as a function of grazing angle, is shown in Fig. 2. Calculations for Fig. 2, and the other figures in this paper, were made using both the matrix inversion and the matrix multiplication type solutions for the bottom loss, discussed earlier. For all models and at all grazing angles the difference between the calculated values of bottom loss by the two methods of solution was less than 0.01 db. The curved line represents the calculated bottom losses and the straight lines connect points which are average values of the experimental losses combined in two-degree intervals. The caps on the vertical lines represent values of bottom loss equal to the mean experimental value plus or minus the standard deviation.

In Fig. 3 a comparison is made between experimental values, averaged over five-degree intervals, and calculated bottom losses for a

two-layer model, the upper layer six feet thick*. This model is listed as Model B in Table 3. A study of Figs. 2 and 3 led to the following conclusions. The broad peaks shown in the experimental losses averaged over five-degree intervals are the result of interference of sound reflected from the surface of the bottom and from the interface at approximately six feet. The rapid fluctuations that appear in the experimental curves averaged over two-degree intervals are probably due to the interference as a result of sound reflecting from the 20-ft deep interface. The large standard deviations of the individual data points are discussed in the following section.

In contrast to Area I, core samples were not taken in Areas II and III. Consequently, the mathematical models of the sediment in these areas are overly simple. The layer constants λ' and μ' were chosen so that the calculated and experimental values of bottom loss would have the same general angular dependence and so the calculated compressional velocity in the layer would have a reasonable value. The attenuation constants were then adjusted for agreement between the experimental and calculated bottom loss curves at small grazing angles.

Area II is deep water area off the California coast. The bottom is believed to be a silty clay. Because a detailed bottom study was not made in this area, a single layer model was chosen for the bottom loss

*Before the present calculations were begun and before core samples in this area were available, Mr. Garland Bernard of the Defense Research Laboratory, Austin, Texas suggested that, on the basis of bottom loss calculations for a two-layer absorbing liquid bottom, the experimental bottom losses were consistent with a discontinuity in the bottom at a depth of six feet. Subsequent core samples proved this to be true.

calculations. The experimental tests in Area II were made at frequencies of 0.7, 1.3, and 3.0 kc. Because the set of measurements at 1.3 kc covered a larger range of grazing angles the model constants were adjusted for this frequency. Theoretical curves at 0.7 and 3.0 kc were then calculated assuming two different frequency variations for the attenuation constant μ'', as explained later. The experimental data indicate rather large overall bottom losses with a maximum bottom loss for the 1.3 kc tests at a grazing angle of approximately 14 degrees. The maximum loss at small grazing angles can be explained by either a low velocity bottom (Model C and Fig. 4) or a highly attenuating bottom (Model F and Fig. 5). In the low velocity cases the high bottom loss is due to refraction of the sound into the bottom, mostly in the form of a compressional wave, while in the high attenuation models the high loss is largely due to conversion of sound energy into a shear wave. That widely differing models can be used to explain the bottom loss curves proves the need for measurements of the physical properties of the bottom, particularly the in situ ratio of the sound velocity in water to the compressional velocity in the upper few feet of sediment. This in situ ratio has been determined in a few cases by Hamilton using the bathyscaph TRIESTE[13].

For both the low velocity models and the high velocity models the attenuation constant μ'' was chosen for a fit of the experimental and calculated bottom loss curves at 1.3 kc. The theoretical loss curves at 0.7 and 3.0 kc are determined by the frequency dependence of μ''.

It seems reasonable that over this frequency range μ'' can be assumed to vary as $\mu'' = \mu''_o \omega^n$, μ''_o equal to a constant and $0 \leq n \leq 1$. For example, if n is 0 the velocities of the compressional and shear waves are independent of frequency and the attenuation of these waves will be linear with frequency. If n is 1, the sediment layers are represented as a Voigt solid type material and the velocity and attenuation relations are more complicated[5].

In this paper, it was assumed alternatively that $\mu'' = \mu''_o \omega$ and $\mu'' = \mu''_o$ (n = 1 or 0). Models C, D, and E (Table 3 and Fig. 4) represent the low velocity case, with $\mu'' = \mu''_o \omega$, at frequencies of 1.3, 0.7, and 3.0 kc respectively. Note that Model E is not a low velocity case since, as a result of the increase in the attenuation constant, the compressional velocity in the sediment is higher than the water velocity. For the assumption $\mu'' = \mu''_o$, the losses are independent of frequency and the bottom loss curves are given by Model C, Fig. 4. Models F, G, and H (Table 3 and Fig. 5) have the same correspondence for the high velocity models.

The experimental losses, as shown in Fig. 4 or 5, do not increase at the higher frequencies, however, it cannot be concluded that the assumption n = 1 is a better choice. At least for many ocean bottoms, the single layer model is a poor representation of the sediment layers, particularly for low frequency bottom loss calculations. A multi- layer model will show a general increase of bottom loss with frequency for

either assumption. It might be noted that the assumption $n = 1$ leads to some unlikely increases of the compressional velocity with frequency (Table 3, Column 9). Also, there are reports on the direct measurement of attenuation constants which indicate that the attenuation terms are independent of frequency[14, 15].

Area III is a deep water area of the Bering Sea. The reflection measurements immediately suggest that the low losses at angles near normal incidence are due to a hard reflecting layer, such as basalt. The larger losses at small grazing angles are most likely due to an absorbing layer, such as silt, lying on top of the hard layer. A two-layer model was used and the attenuation of the upper layer was adjusted to fit the peak of the experimental curve at the 1.3 kc frequency (Fig. 6). In Fig. 7 the 1.3 kc curve is repeated along with experimental and calculated curves for the bottom loss at 0.7 kc. The 0.7 kc curves were calculated assuming μ'' to be constant and then to be a linear function of frequency. The agreement with experimental values is only fair for either curve. Experimental data at 3.0 kc were not obtained in this area.

SOME COMMENTS ON THE FLUCTUATIONS OF THE BOTTOM LOSSES

Fluctuations in the intensity of bottom reflected sound are usually attributed to interference of signals traveling along different paths, or scattered from reflecting objects lying on the bottom, or scattered from reflecting facets of the surface of the bottom. In the areas discussed

in this paper, the water-sediment interfaces are relatively smooth so that it was expected that fluctuations of the bottom loss would be small.

Standard deviations, averaged over all grazing angles, of the bottom loss measurements in Area II were 3.8, 3.2 and 3.3 db at frequencies of 0.7, 1.3, and 3.0 kc respectively. In Area III the standard deviations of the bottom loss were 2.4 db at 1.3 kc and 1.6 db at 0.7 kc. In the deep water areas (II and III) shallow source and receiver depths and long pulse length (0.5 sec) signals were used. The fluctuations result, most probably, from scattering and from mutual interference of the four possible signal paths having a single bottom reflection, which are described in the Appendix. In moderate seas the surface motion of the water will cause the difference in path lengths of the four signals to vary by more than a wavelength at these frequencies. Thus, between successive pings the phase differences of the four signals will change in a random manner.

Results from the Appendix show that a standard deviation of about 2.3 db is expected because of four-path interference of constant amplitude signals in Areas II and III. Since each of the four signals will have some individual amplitude fluctuation the actual four-path interference should be somewhat larger. Thus it seems that in Area II a large part of the observed fluctuations is due to four-signal interference and in Area III almost all of the variation in bottom loss was due to this effect. The low value of fluctuation (1.6 db) at 0.7 kc in Area III can be explained by noting that these tests were made in unusually calm seas and that at the

0.7 kc frequency the phase differences betwen the interfering signals were not random.

The experimental losses in Area I were measured in 14 different tests made over a period of several months. Thus the losses reported for a certain grazing angle were obtained at several locations in the same general area. Because of this, and apparently because of the strong interference of sound reflecting from different surfaces of the sediment layers, the fluctuations of the bottom loss were large in this area. The standard deviation was 4.4 db when the losses were grouped in two-degree intervals and 4.9 db when taken in five-degree intervals. Smaller samples of data also showed considerable fluctuation.

CONCLUSION

Equations have been derived, in two different forms, for the calculation of the bottom loss of a plane sound wave in water and incident on an arbitrary number of visco-elastic solid layers. Thus the model includes the effects of sediment layering, the absorption of sound waves in the bottom sediments, and the generation of shear waves at the interfaces. In most of the models considered, the bottom losses were high at small grazing angles because of a large part of the sound energy being converted into a shear wave.

The bottom loss as a function of grazing angle is calculated for two locations off the California coast and at a deep water location in the Bering Sea. In only one of these locations was more than half of the bottom constants, required to define the model bottom, available. Thus, no claim can be made about how well this model will represent an ocean bottom, even in the special case where the interfaces are smooth and the layering uniform. At one location 4 core samples were available so that the most critical assumptions were the values of the layer attenuation constants. The chosen values of these constants were in general agreement, assuming a linear relation of attenuation to frequency, to those determined at high frequencies for similar sediments by the resonance method.

Fluctuations in the bottom loss at the deep water locations are most readily explained as resulting from interference of the four signals with one bottom reflection. The large fluctuation in the bottom loss in the moderate depth water location is most probably the result of combining experimental measurements from slightly displaced stations in an area where there are strong but somewhat irregular scattering surfaces.

REFERENCES

1. E.g., J. C. Fry and R. W. Raitt, "Sound Velocities at the Surface of Deep Sea Sediments," J. of Geophys. Res. 66, 589 (1961)

2. E.g., C. L. Pekeris, "Propagation of Explosive Sound in Shallow Water," Geol. Soc. Amer. Mem. 27: Propagation of Sound in the Ocean, 2nd Sec. (1948)

3. K. V. Mackenzie, "Reflection of Sound from Coastal Bottoms," J. Acoust. Soc. Amer. 32, 221 (1960)

4. T. G. Bell, "Reflection and Scattering of Sound by the Sea Bottom, Field Data," Paper presented at the 68th Meeting of the Acoust. Soc. Amer., (Oct. 1964)

5. H. P. Bucker, "Normal-Mode Sound Propagation in Shallow Water," J. Acoust. Soc. Amer. 36, 251 (1964)

6. Maurice Ewing, W. S. Jardetsky and F. Press, Elastic Waves in Layered Media (McGraw Hill book Co., Inc., New York, 1957), pp 74-89

7. Reference 6, p 76

8. W. T. Thomson, "Transmission of Elastic Waves through a Stratified Solid Material," J. Appl. Phys. 21, 89 (1950)

9. D. G. Moore, private communication

10. George Shumway, "Sound Speed and Absorption Studies of Marine Sediments by a Resonance Method," Geophysics 25, 451, 659 (1960)

11. E. L. Hamilton, G. Shumway, H. W. Menard, and C. J. Shipek, "Acoustical and Other Physical Properties of Shallow Water Sediments off San Diego," J. Acoust. Soc. Amer. 28, 1 (1956)

12. A. B. Wood and D. E. Weston, "The Propagation of Sound in Mud," Acustica, 14, 156 (1964)

13. E. L. Hamilton, "Sediment Sound Velocity Measurements Made In Situ from Bathyscaph TRIESTE," J. of Geophys. Res. 68, 5991 (1963)

14. Francis Birch, ed. Handbook of Physical Constants, Geol. Soc. Amer. Special Paper No. 36; (1953)

15. D. E. Weston, "On the Frequency Independence of the Acoustic Loss Factor in Earth Materials," Geophys. J. Of the Royal Astron. Soc. 8, 269 (1963)

16. Lord Rayleigh (J. W. Strutt), "On the Problem of Random Vibrations, and of Random Flights in One, Two, or Three Dimensions," Philosophical Magazine 37, 321 (1919)

17. Karl Pearson, "A Mathematical Theory of Random Migration," Drapers Co., Research Memoirs, Biometric Series III (Cambridge Univ. Press, London, 1906)

18. W. R. Bennett, "Distribution of the Sum of Randomly Phased Components," Quart. Appl. Math. 5, 385 (1948)

Appendix

In the deep water areas (II and III) discussed in this report, the source and receiver were both located at shallow depths and 0.5 sec pulses were used. Under these conditions the four signals that have one bottom reflection will overlap. Let the signal that is reflected from only the bottom be labeled as B, the signal reflected from the surface and then the bottom be called S-B, etc. Because the source and receiver were located at nearly equal depths the S-B and B-S paths have almost equal travel times. Then the signal recorded, during the arrival of the four single bottom reflected paths will at increasing times be made up of the following five combinations:

1. B
2. B, S-B, B-S
3. B, S-B, B-S, S-B-S
4. S-B, B-S, S-B-S
5. S-B-S.

In the analysis of the experimental records the peak value of the recorded signal was measured which may occur in any of five possible combinations of signals. Let $f_i(p)dp$ be the probability of finding a value of peak pressure between the values of p to $p+dp$ in the i^{th} combination of signals. Then the probability of finding the largest value of peak pressure from any of the five combinations to be between the values p to $p+dp$ is

$$F_5(p) = \sum_{i=1}^{5} \left\{ f_i(p) \prod_{j=1 \neq i}^{5} \int_0^p f_j(p')dp' \right\}$$

It is assumed now that each of the four interfering signals has constant amplitude and that the phase differences between the interfering signals are random. The distribution functions f_1 and f_5 are Dirac delta-functions. The distribution functions for the three interfering signals (f_2 and f_4) can be written as complete elliptic integrals of the first type.[16]

Let the B, S-B, B-S, and S-B-S signals have the respective peak amplitudes of 1, $\underline{a}$, $\underline{a}$, and $\underline{a}^2$, where $\underline{a} \leq 1$. Then f_2 is the distribution function of the peak amplitudes 1, $\underline{a}$, and $\underline{a}$ combining with random phase. Fig. 8 is a graph of f_2 for values of the parameter $\underline{a}$ equal to 1.0, 0.8, and 0.6.

The function f_3, which represents the combination of all four signals, was calculated, following the method of Pearson[17], by numerical integration of a distribution function for three signals. Fig. 9 is a graph of f_3 for values of $\underline{a}$ equal to 1.0, 0.8, and 0.6. The functions f_2, f_3, and f_4 can also be calculated in terms of an infinite integral or as an infinite series[18]. These methods were not used here because of their slow convergence when the number of combining signals is small.

The desired function F_5 is easily calculated when f_2, f_3, and f_4 are known. Fig. 10 is a graph of F_5 for values of $\underline{a}$ equal to 1.0, 0.8, and 0.6. From F_5 the distribution function of the bottom loss can be calculated. Although the value of the bottom loss (in db) depends upon the reference intensity the standard deviation of the bottom loss does not. The expected standard deviation of the bottom loss, for the above assumptions,

as a result of four-signal interference is 2.4 db for $\underline{a} = 1.0$, and 2.3, 2.2, 2.1, and 2.0 db for values of $\underline{a}$ equal to 0.9, 0.8, 0.7, and 0.6.

ACKNOWLEDGMENTS

The general direction for this work was provided by Mr. F. E. Hale, Head of the Sound Propagation Division at NEL. At-sea measurements, described in Part I, were directed by Messrs. Henry Westfall and W. E. Batzler. Dr. E. L. Hamilton provided useful information and ideas concerning the bottom constants used in Part II.

$$\begin{bmatrix} ik\cos P & k\sin P & -ikb_n\cos Q & -kb_n\sin Q \\ ka_n\sin P & ika_n\cos P & k\sin Q & ik\cos Q \\ -i\frac{\mu_n k^2}{\omega}(b_n^2-1)\cos P & -\frac{\mu_n k^2}{\omega}(b_n^2-1)\sin P & -i2\frac{\mu_n k^2}{\omega}b_n\cos Q & -2\frac{\mu_n k^2}{\omega}b_n\sin Q \\ -2\frac{\mu_n k^2}{\omega}a_n\sin P & -i2\frac{\mu_n k^2}{\omega}a_n\cos P & \frac{\mu_n k^2}{\omega}(b_n^2-1)\sin Q & i\frac{\mu_n k^2}{\omega}(b_n^2-1)\cos Q \end{bmatrix}$$

$P = ka_n d_n$, $\quad Q = kb_n d_n$.

TABLE I. ELEMENTS OF THE MATRIX M_n^n

TABLE 2. ELEMENTS OF D_n MULTIPLIED BY $(b_n^2 + 1)$

$$(11) = \left[2\cos P + (b_n^2 - 1)\cos Q\right]$$

$$(12) = -i\left[\frac{b_n^2 - 1}{a_n}\sin P - 2b_n \sin Q\right]$$

$$(13) = \frac{\omega}{\mu_n k}\left[\cos Q - \cos P\right]$$

$$(14) = \frac{i\omega}{\mu_n k}\left[\frac{1}{a_n}\sin P + b_n \sin Q\right]$$

$$(21) = -i\left[2a_n \sin P - \frac{b_n^2 - 1}{b_n}\sin Q\right]$$

$$(22) = \left[(b_n^2 - 1)\cos P + 2\cos Q\right]$$

$$(23) = \frac{i\omega}{\mu_n k}\left[a_n \sin P + \frac{1}{b_n}\sin Q\right]$$

$$(24) = \frac{\omega}{\mu_n k}\left[\cos Q - \cos P\right]$$

$$(31) = 2\frac{\mu_n k}{\omega}(b_n^2 - 1)\left[\cos Q - \cos P\right]$$

$$(32) = i\frac{\mu_n k}{\omega}\left[\frac{(b_n^2 - 1)^2}{a_n}\sin P + 4b_n \sin Q\right]$$

$$(33) = \left[(b_n^2 - 1)\cos P + 2\cos Q\right]$$

$$(34) = -i\left[\frac{b_n^2 - 1}{a_n}\sin P - 2b_n \sin Q\right]$$

$$(41) = i\frac{\mu_n k}{\omega}\left[4a_n \sin P + \frac{(b_n^2 - 1)^2}{b_n}\sin Q\right]$$

$$(42) = 2\frac{\mu_n k}{\omega}(b_n^2 - 1)\left[\cos Q - \cos P\right]$$

$$(43) = -i\left[2a_n \sin P - \frac{b_n^2 - 1}{b_n}\sin Q\right]$$

$$(44) = \left[2\cos P + (b_n^2 - 1)\cos Q\right]$$

$P = k a_n d_n$, $Q = k b_n d_n$.

Table 3

TABLE OF BOTTOM CONSTANTS (ENGLISH UNITS $lb_m - ft - sec$)

MODEL & AREA (1)	FREQ (KC) (2)	WATER VELOCITY (3)	LAYER NO. ① (4)	λ' ② (5)	$\frac{\mu'}{\lambda'}$ (6)	μ'' ② (7)	LAYER THICKNESS (8)	COMPRESSIONAL VELOCITY (9)	ATTEN. OF COMP. WAVE ③ (10)	DENSITY (11)
A (I)	1.5	4885	4	2.30 x 9	.01	8x7	1	4776	.39	103
			3	2.37 x 9	.1	3x7	5	5051	.12	112
			2	2.53x 9	.2	6x6	14	5412	.02	121
			1	6.00x 9	.4	4x6	∞	8980	—	134
B (I)	1.5	4885	2	2.8x 9	0	1 x 8	6	5015	.39	112
			1	3.5x 9	0	1 x 7	∞	5380	.03	121
C (II)	1.3	4970	1	3.0 x 9	.01	3.0x8	∞	4880	.9	130
D (II)	0.7	4970	1	3.0x 9	.01	1.6x 8	∞	4860	.3	130
E (II)	3.0	4970	1	3.0 x 9	.01	6.9x 8	∞	5010	2.3	130
F (II)	1.3	4970	1	3.0x 9	.01	1.0 x 9	∞	5500	5.4	130
G (II)	0.7	4970	1	3.0x 9	.01	5.4x8	∞	5320	.7	130
H (II)	3.0	4970	1	3.0x9	.01	2.3x9	∞	6430	9.5	130
I (III)	1.3	4980	2	2.25x9	.01	1 x 8	3	4800	.4	100
			1	4.30x10	1.0	1 x 6	∞	25,900	–	192
J (III)	0.7	4980	2	2.25 x 9	.01	5.4 x 7	3	4790	.1	100
			1	4.30 x 10	1.0	5.4 x 5	∞	25,900	–	192
K (III)	0.7	4980	2	2.25 x 9	.01	1 x 8	3	4790	.2	100
			1	4.30 x10	1.0	1 x 6	∞	25,900	–	192

① Layer 1 is the deepest layer

② $2.30 \times 9 \equiv 2.30 \times 10^9$

③ Attenuation of a plane compressional wave in db/ft

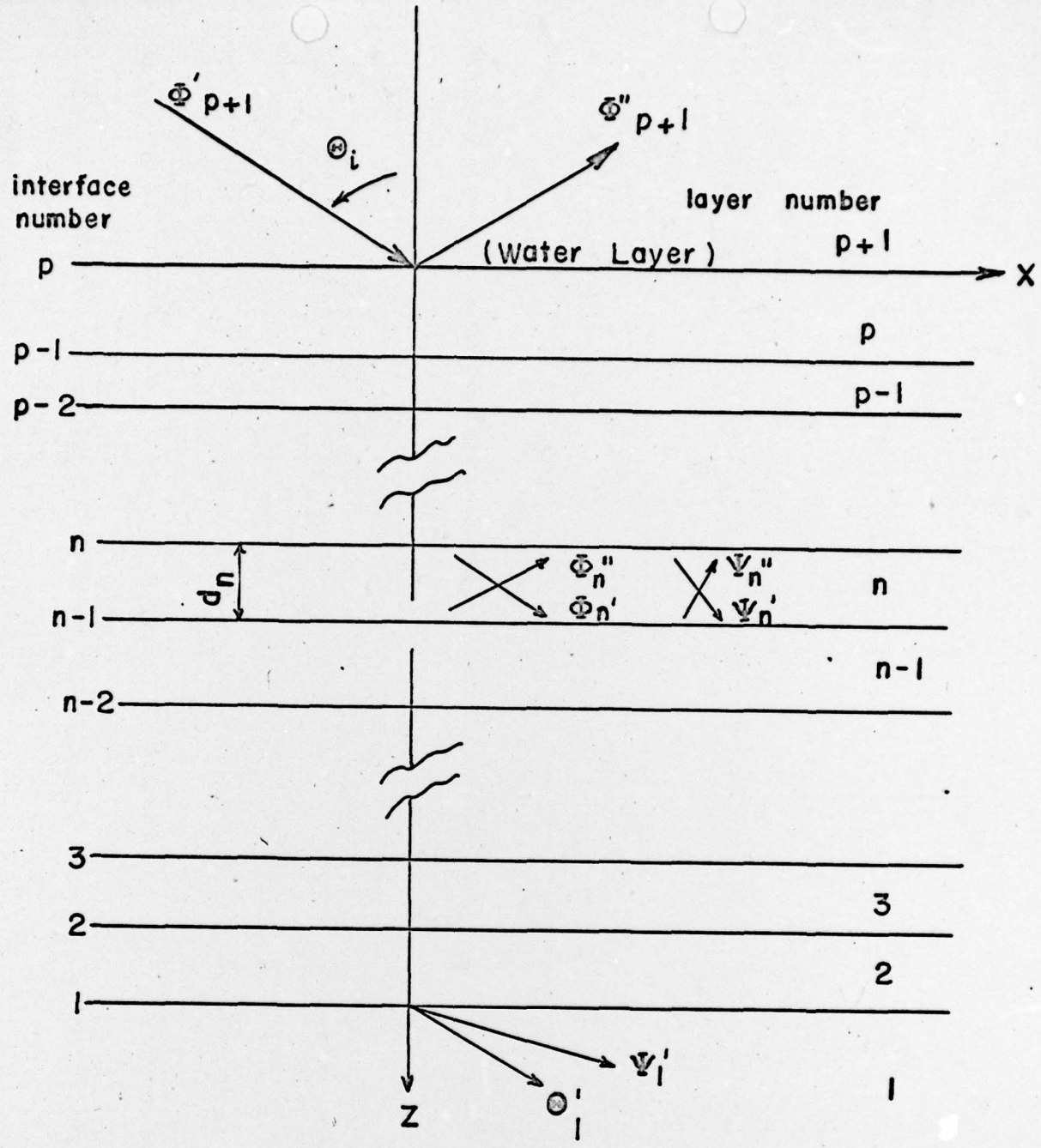

Fig.1

VELOCITY POTENTIAL FUNCTIONS IN THE MODEL BOTTOM

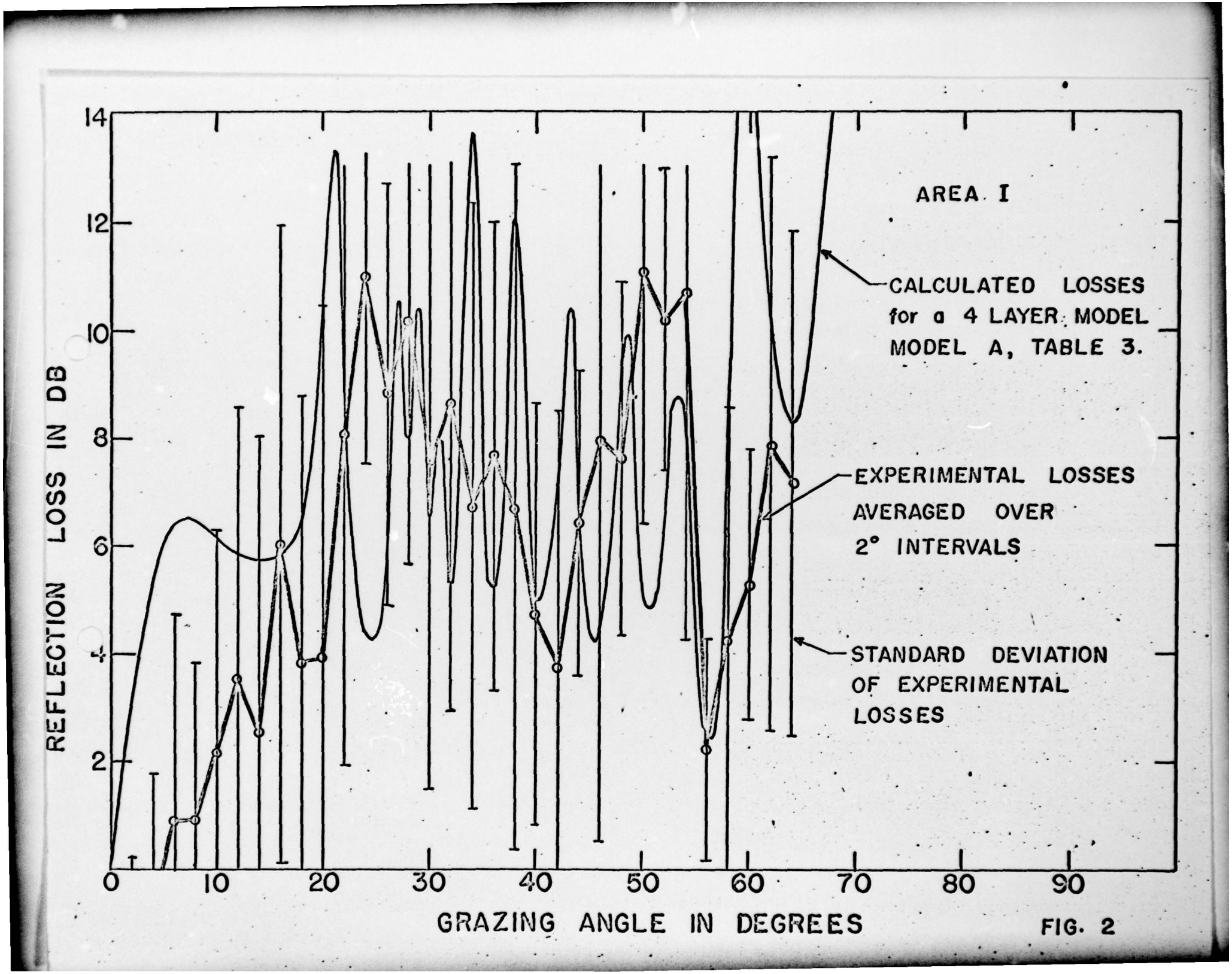
AREA I
CALCULATED LOSSES for a 4 LAYER MODEL MODEL A, TABLE 3.
EXPERIMENTAL LOSSES AVERAGED OVER 2° INTERVALS
STANDARD DEVIATION OF EXPERIMENTAL LOSSES
REFLECTION LOSS IN DB
GRAZING ANGLE IN DEGREES
0
10
20
30
40
50
60
70
80
90
2
4
6
8
10
12
14

FIG. 2

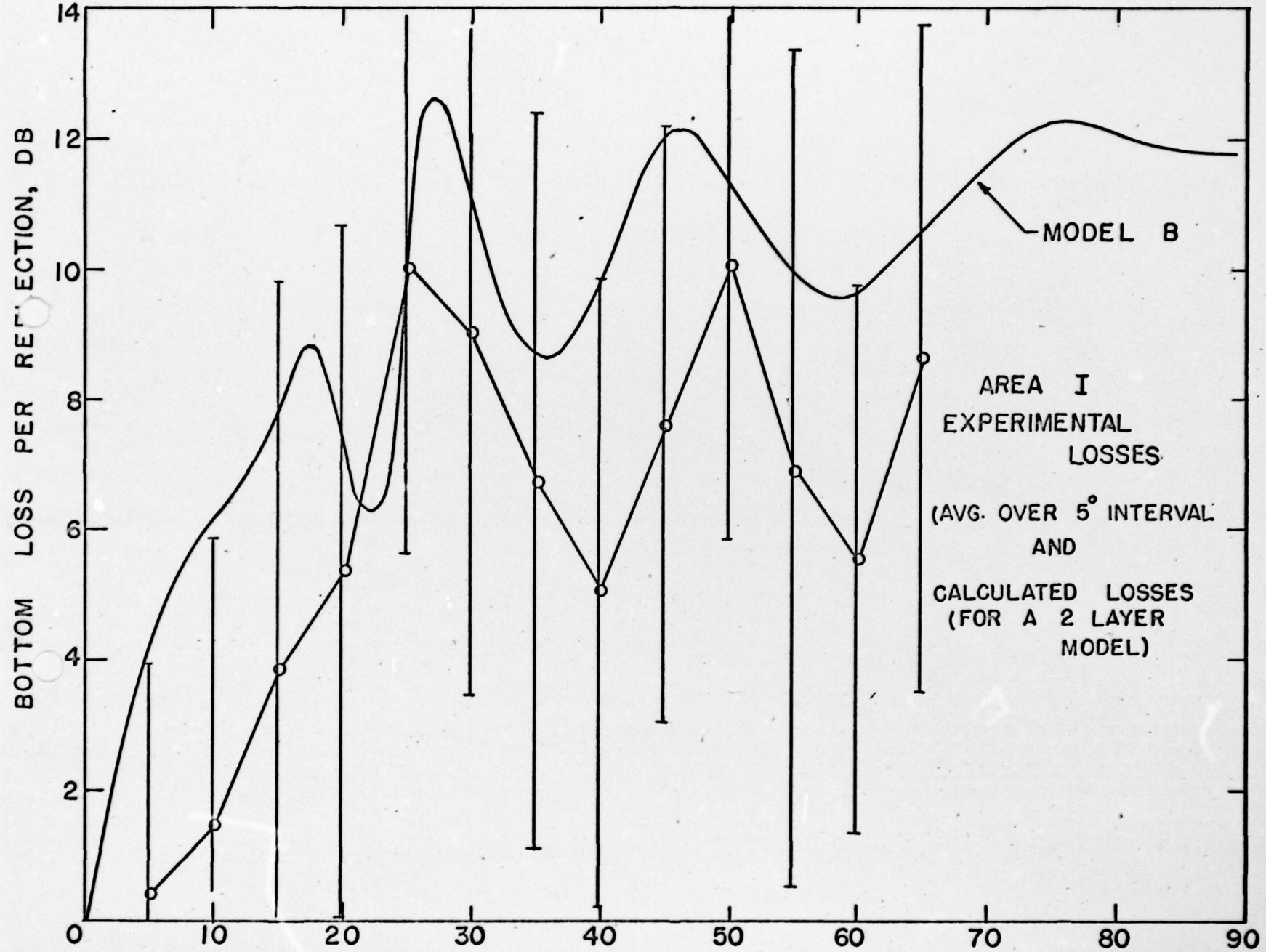
BOTTOM LOSS PER REFLECTION, DB
14
12
10
8
6
4
2
0
10
20
30
40
50
60
70
80
90
GRAZING ANGLE, DEGREES
MODEL B
AREA I
EXPERIMENTAL
LOSSES
(AVG. OVER 5° INTERVAL
AND
CALCULATED LOSSES
(FOR A 2 LAYER
MODEL)

FIG. 3

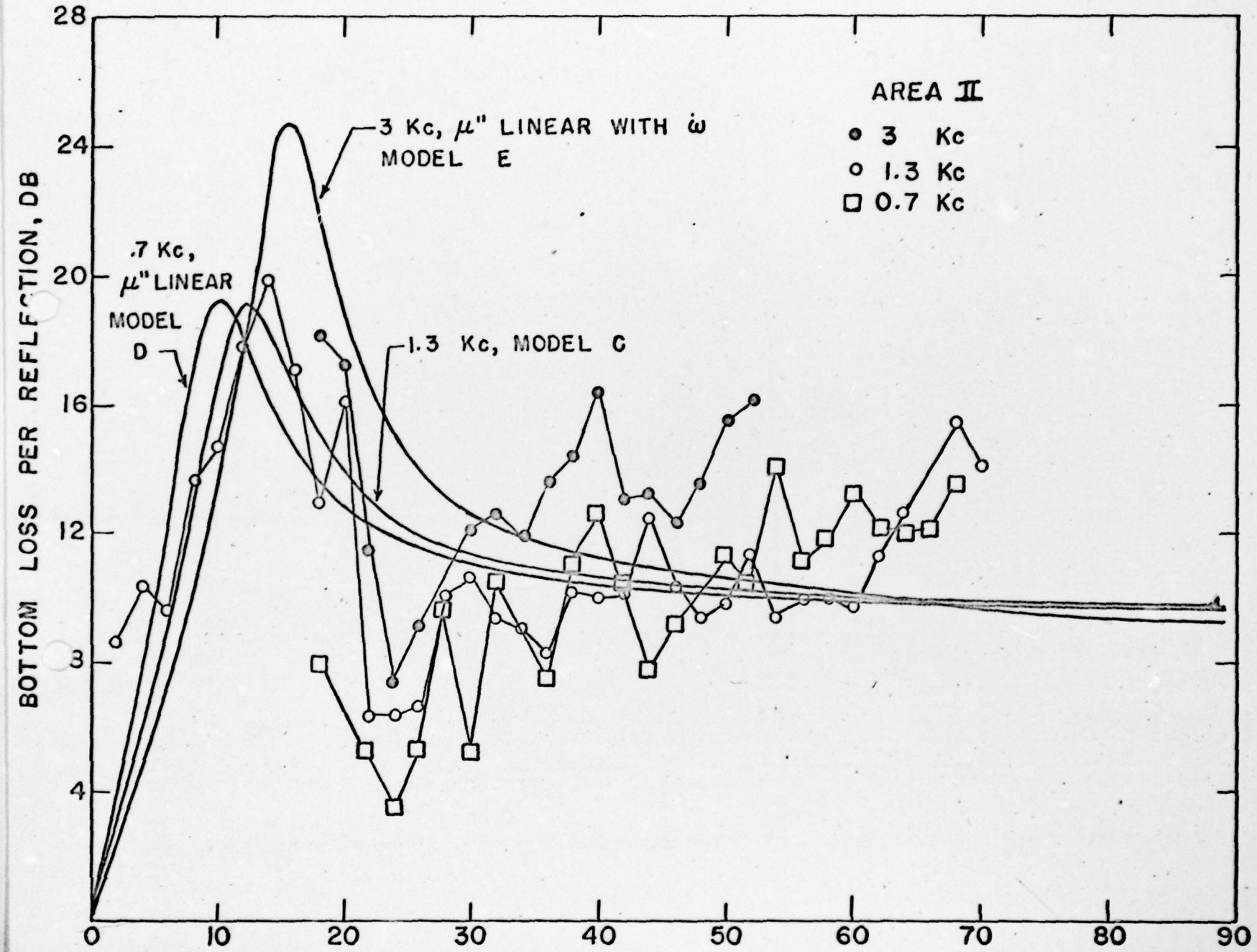
AREA II
3 Kc
1.3 Kc
0.7 Kc
3 Kc, μ" LINEAR WITH ω
MODEL E
.7 Kc,
μ" LINEAR
MODEL
D
1.3 Kc, MODEL C
BOTTOM LOSS PER REFLECTION, DB
GRAZING ANGLE, DEGREES
28
24
20
16
12
3
4
0
10
20
30
40
50
60
70
80
90

FIG. 4

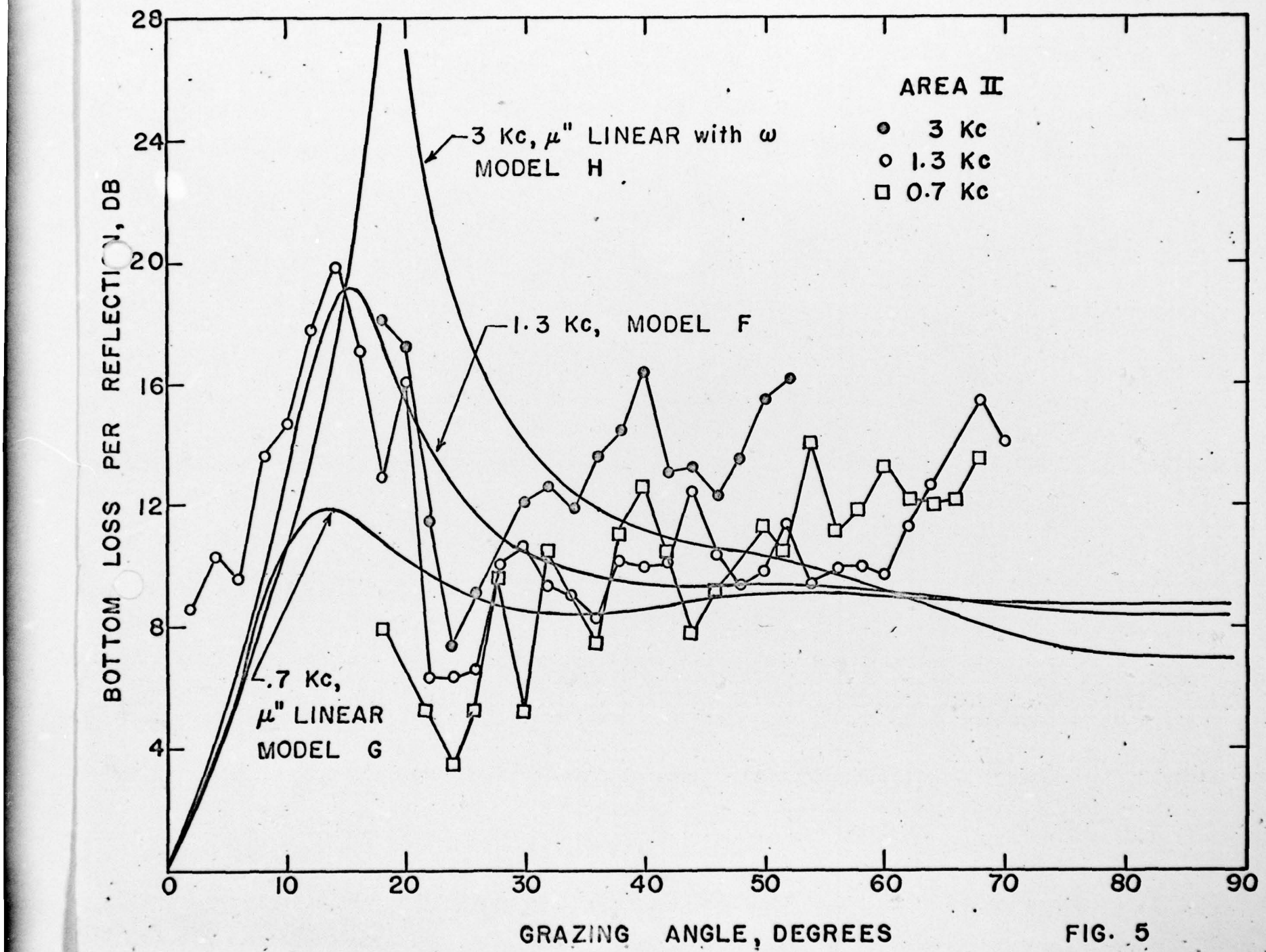
AREA II
3 Kc
1.3 Kc
0.7 Kc
3 Kc, μ" LINEAR with ω
MODEL H
1.3 Kc, MODEL F
.7 Kc,
μ" LINEAR
MODEL G
BOTTOM LOSS PER REFLECTION, DB
GRAZING ANGLE, DEGREES
0
10
20
30
40
50
60
70
80
90
4
8
12
16
20
24
28

FIG. 5

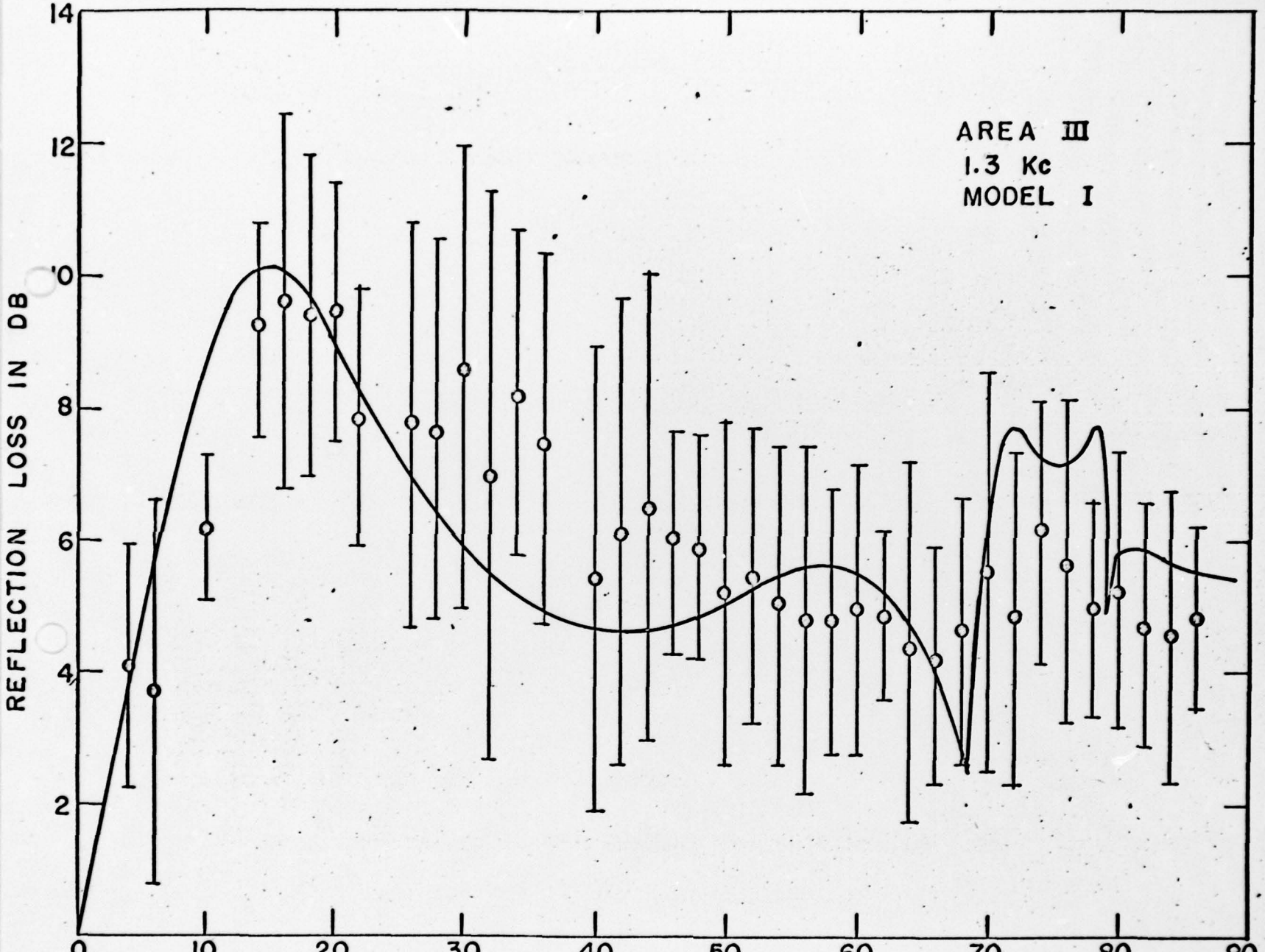
AREA III
1.3 Kc
MODEL I
REFLECTION LOSS IN DB
GRAZING ANGLE IN DEGREES
0
10
20
30
40
50
60
70
80
90
2
4
6
8
10
12
14

FIG. 6

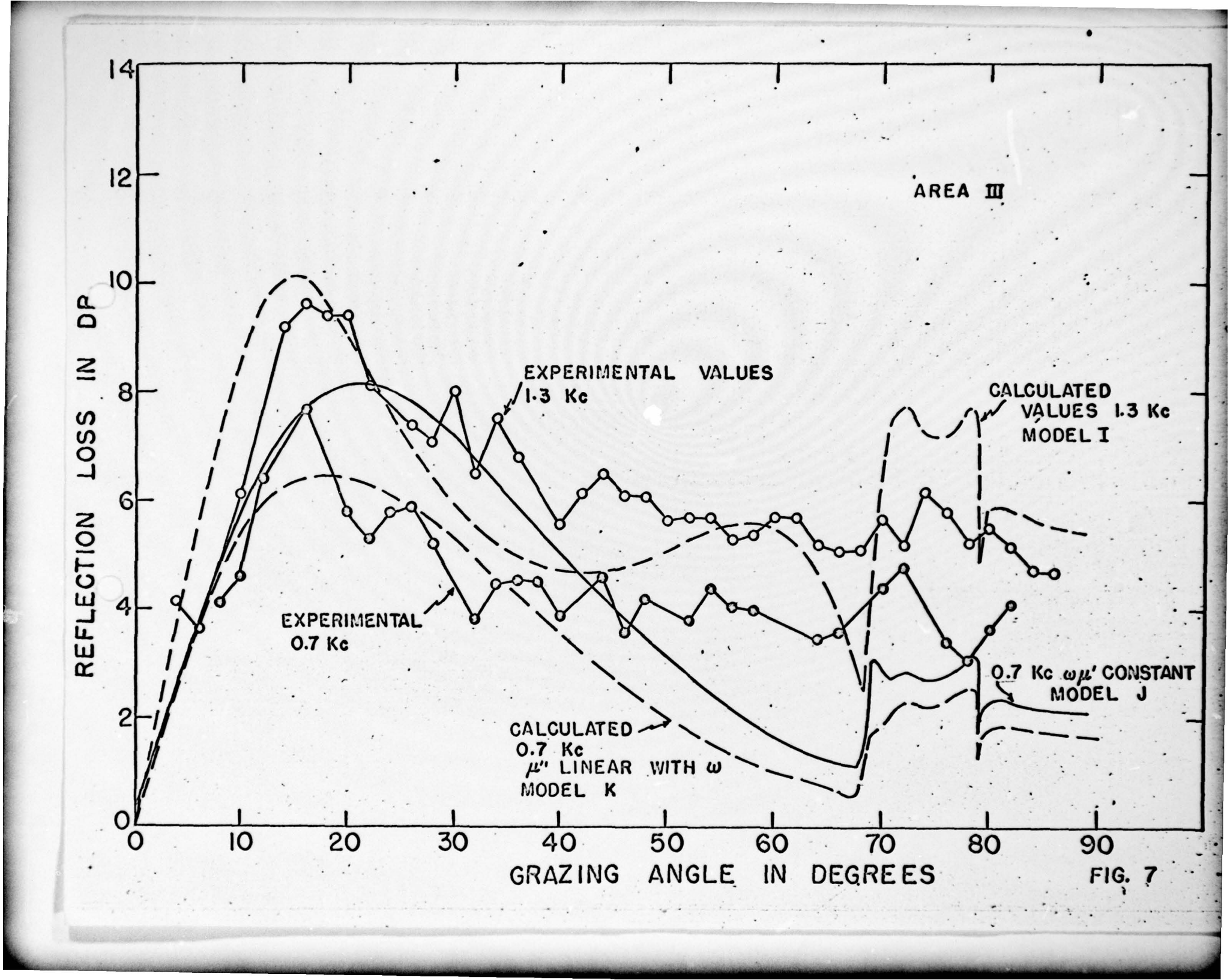
AREA III
REFLECTION LOSS IN DP
GRAZING ANGLE IN DEGREES
EXPERIMENTAL VALUES
1.3 Kc
CALCULATED
VALUES 1.3 Kc
MODEL I
EXPERIMENTAL
0.7 Kc
0.7 Kc ωμ' CONSTANT
MODEL J
CALCULATED
0.7 Kc
μ'' LINEAR WITH ω
MODEL K
0
2
4
6
8
10
12
14
0
10
20
30
40
50
60
70
80
90

FIG. 7

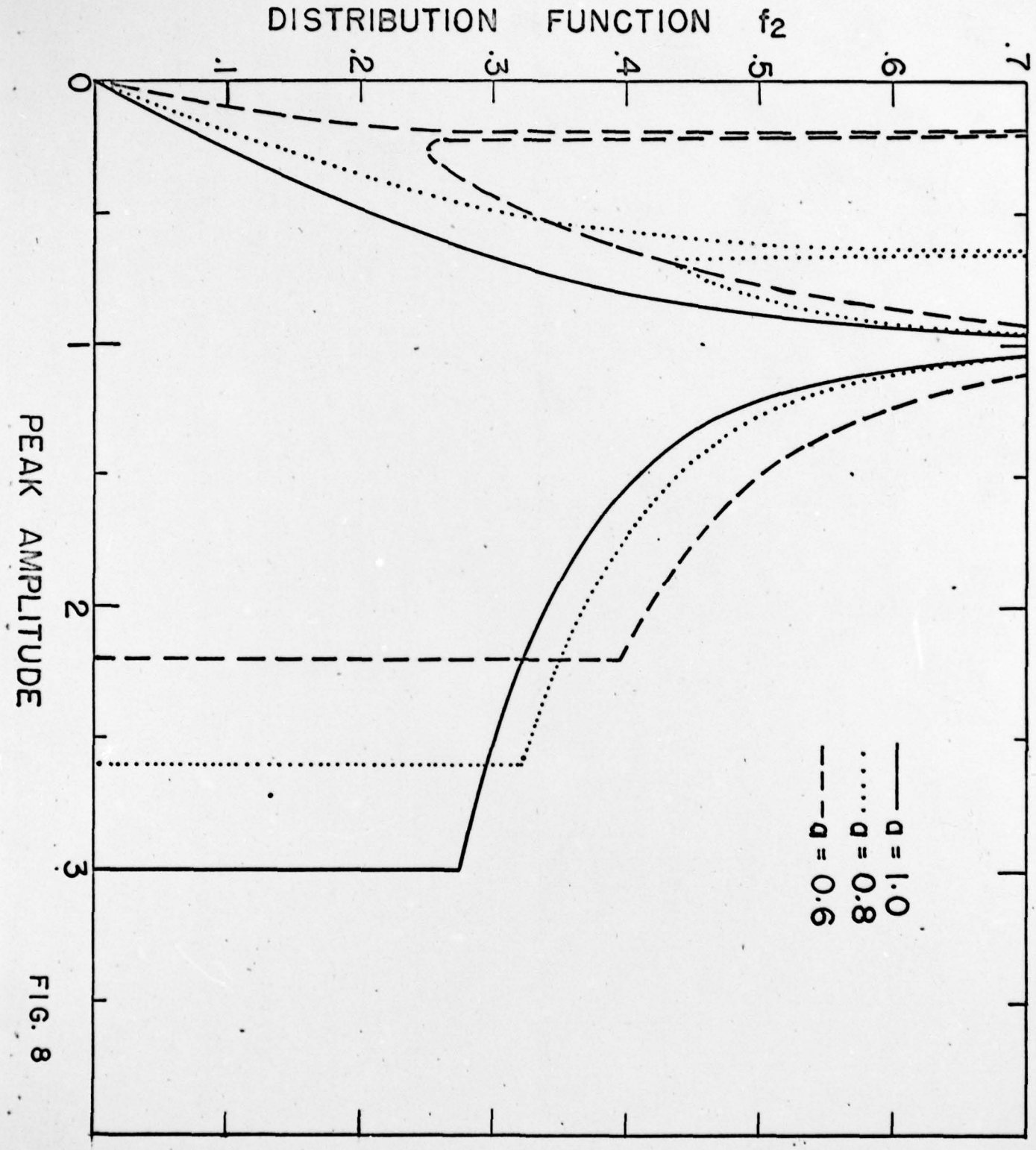
DISTRIBUTION FUNCTION f_2
.1
.2
.3
.4
.5
.6
.7
0
1
2
3
PEAK AMPLITUDE
a = 1.0
a = 0.8
a = 0.6

FIG. 8

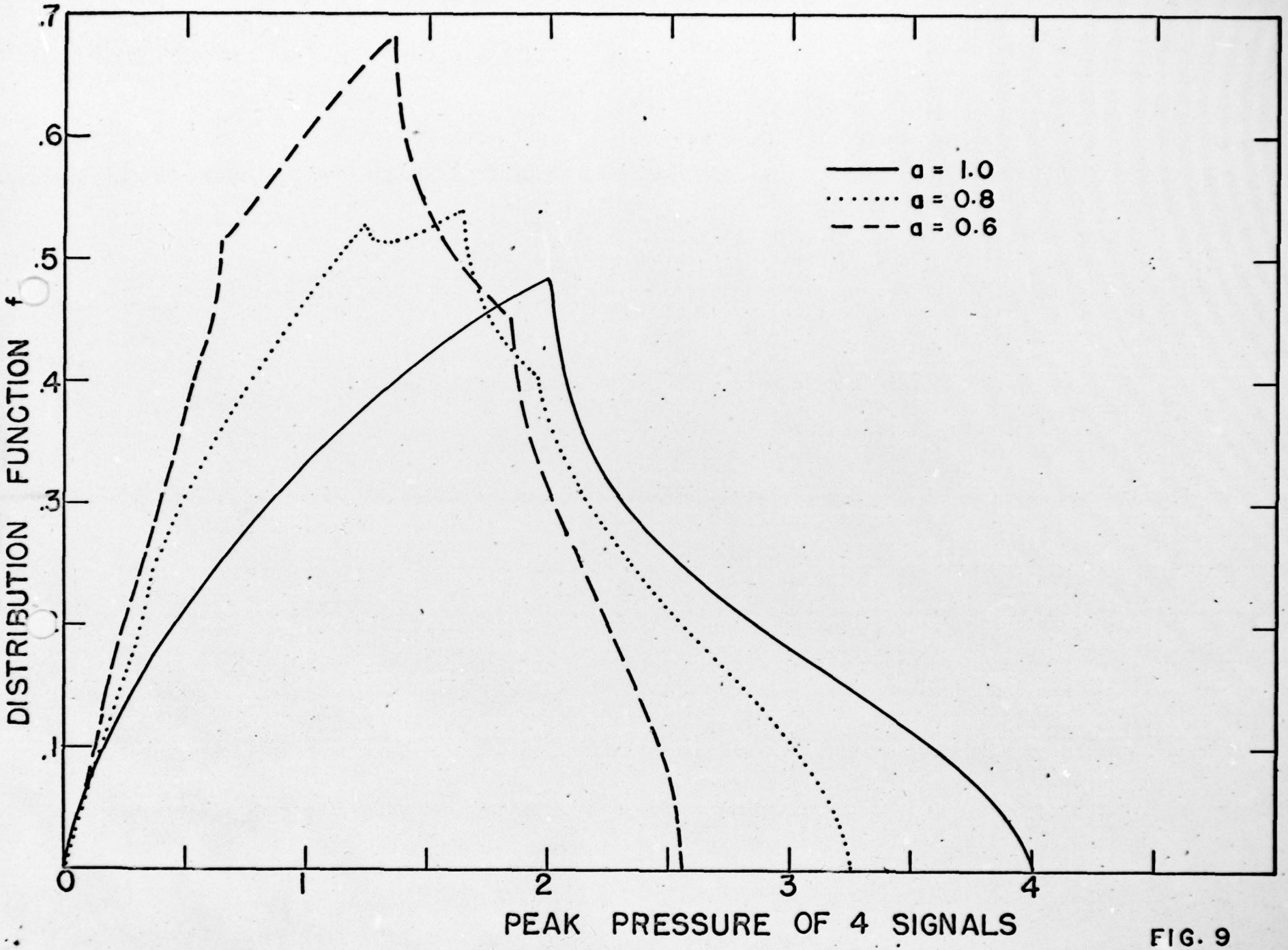
.7
.6
.5
.4
.3
.1
DISTRIBUTION FUNCTION f
a = 1.0
a = 0.8
a = 0.6
0
1
2
3
4
PEAK PRESSURE OF 4 SIGNALS

FIG. 9

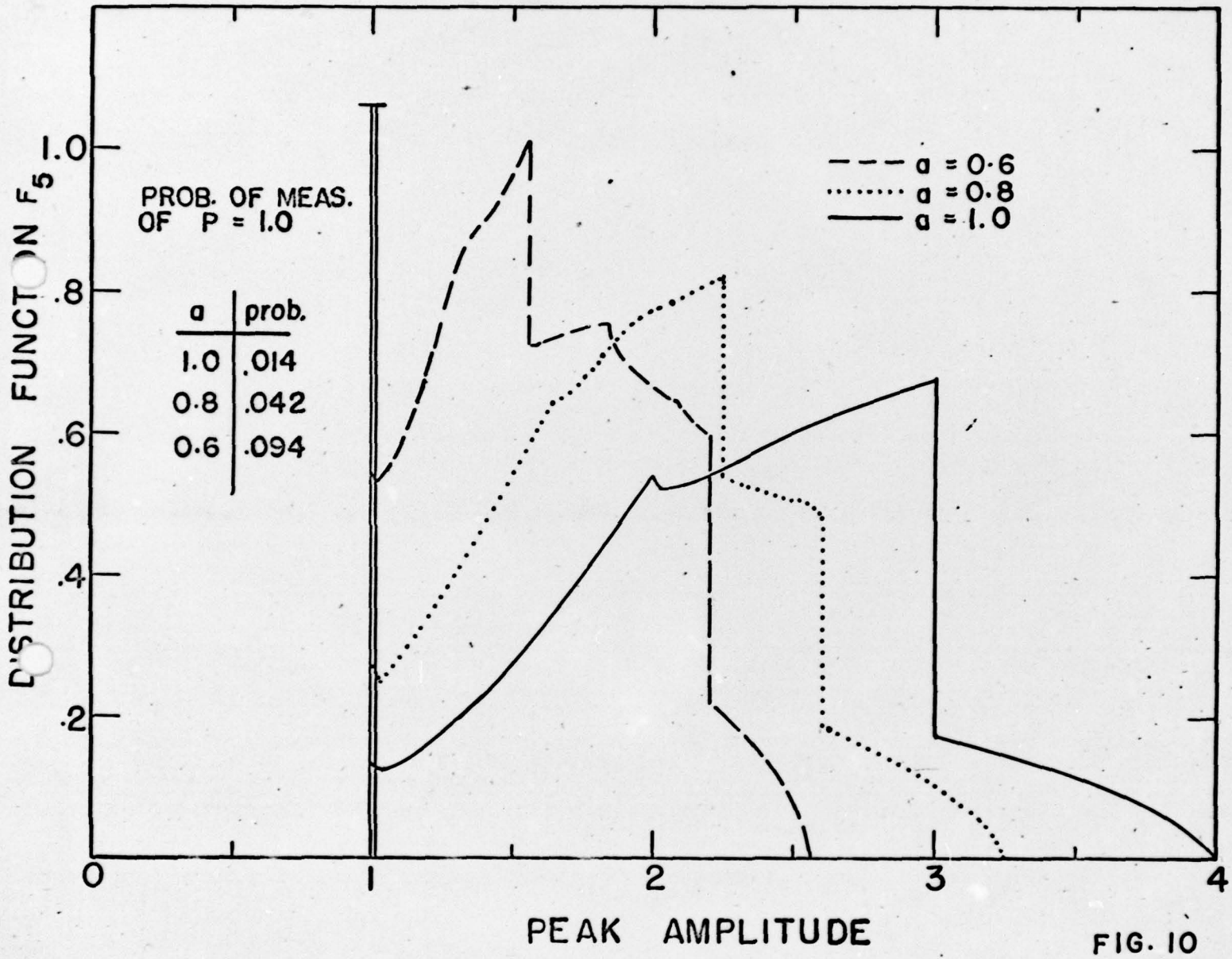
DISTRIBUTION FUNCTION F_5
1.0
.8
.6
.4
.2
0
1
2
3
4
PEAK AMPLITUDE
PROB. OF MEAS. OF P = 1.0
a | prob.
1.0 | .014
0.8 | .042
0.6 | .094
a = 0.6
a = 0.8
a = 1.0

FIG. 10